17th World Conference on Earthquake Engineering, 17WCEE

Sendai, Japan - September 13th to 18th 2020

Post-Fracture Performance Assessment of the Cast Steel Yielding Connector in Non-Buckling Concentrically Braced Frame

C. Zhong[1], J. Binder[2], M.G. Gray[3], O. Kwon[4], and C. Christopoulos[5]

[1] *Ph.D. Candidate, Department of Civil and Mineral Engineering, University of Toronto, myron.zhong@mail.utoronto.ca*

[2] *Project Engineer, Research and Development, Cast Connex Corporation, j.binder@castconnex.com*

[3] *Executive Vice President, Cast Connex Corporation, m.gray@castconnex.com*

[4] *Associate Professor, Department of Civil and Mineral Engineering, University of Toronto, os.kwon@utoronto.ca*

[5] *Professor, Department of Civil and Mineral Engineering, University of Toronto, c.christopoulos@utoronto.ca*

Abstract

The cast steel Yielding Connector (YC) is a device designed to act as yielding fuse to dissipate earthquake energy through inelastic deformations in specially designed distributed yielding regions, while ensuring controlled elastic response elsewhere in the structure. Typically, the YC is designed for use in highly ductile non-buckling concentrically braced frame systems, or as a damper in other configurations. The YC exhibits a stable, symmetric hysteretic response with a characteristic post-yield stiffness increase due to a combination of friction and second-order geometric effect. The ultimate limit state of the YC is typically governed by ultralow-cycle fatigue (ULCF) fracture of the yielding sections, where fracture begins after a relatively low number of large inelastic cycles, followed by a slow strength degradation for each additional cycle. This paper presented the calibration results of a state-of-art ULCF fracture criteria, the Stress Weighted Damage Model (SWDM) to the cast steel material in the YC by performing a series of notched coupon tests. This SWDM fracture criteria was used in advanced finite element analyses to simulate the entire fracture process of previously tested full-scale YC specimens. Detailed finite element models of YCs were developed to numerically simulate the ductile fracture initiation, propagation and the associated strength degradation due to fracture. Full-scale experimental test results were used to validate the fracture simulation model that employed the calibrated SWDM fracture criteria. Use of the calibrated fracture simulation model for YCs was then presented as an evaluation tool to numerically assess the ultimate performance of structures designed with YC-equipped non-buckling braces under earthquake ground motions. A six-story sample structure was capacity designed with YC-equipped braces. Advanced finite element model of this sample structure was constructed in ABAQUS *explicit*, with YCs modelled in detailed with solid elements and the rest of the structure with beam elements. This model was used in nonlinear time history analyses with a set of sixteen ground motions scaled to the Design Earthquake and Maximum Considered Earthquake seismic hazard levels, to examine the effects of YC's post-yield stiffness and post-fracture strength on the collapse performance of the YC-equipped structure. The results suggested that, with proper capacity design, YC-braced frames exhibited lower likelihood of structural collapse during a significant earthquake event.

Keywords: Cast Steel Yielding Fuse, Ultralow-Cycle Fatigue, Non-Buckling Braced Frame, Full-Scale Test, Finite Element

1. Introduction

The cast steel Yielding Connector (YC) is a compact seismic energy dissipation device that exhibits large ductility through hysteretic yielding of specially designed distributed yielding regions within the device, therefore ensuring elastic response elsewhere in the structure. The cast steel YC can be employed in highly ductile non-buckling concentrically braced frame systems to provide controllable ductility and energy dissipation in the event of an earthquake. Fig. 1 illustrates the main components of the YC. A set of triangular cast steel yielding fingers, as highlighted in Fig. 1, dissipates energy through simultaneous yielding along the finger length. The elastic arms then transfer loads from the yielding fingers to the connecting brace while remaining elastic. The eccentric load transfer is internally balanced by cover plates connecting elastic arms on both sides to achieve primarily axial loading in the direction of the brace axis. The splice plate assembly with slotted bolted connections transfers axial loads in the direction of the brace axis from ends of yielding fingers to the gusset plate while allowing bolts to slide along the slots to accommodate finger deformations.

The behavior of YC has been extensively evaluated through full-scale experiments and advanced nonlinear finite element (FE) modeling, with a focus on its Ultra-Low-Cycle Fatigue (ULCF) response [1, 2, 3, 4, 5]. Hybrid simulation method has also been used to investigate the global performance of a four-storey YC-braced frame, with the response of the YC-braces being captured physically while the rest of the structure modelled numerically [6]. Recent studies by Zhong et al. [4, 5] presents experimentally validated improvements of ULCF model calibration and FE modeling for YC that extend the numerical simulation of YC to capture its entire ductile fracture process, acknowledging the experimental observation that YC typically exhibits a significant amount of ductility even after local fracture initiation. The use of the improved models in numerically investigating aspects of the YC-equipped braces has also been discussed by Zhong et al. [5]. In this study, the developed models are utilized further to investigate the global responses of a sample six-story non-buckling concentrically braced frames designed with YC-equipped braces, with a focus on the effect of the post-yielding response and gradual capacity degradation of YC.

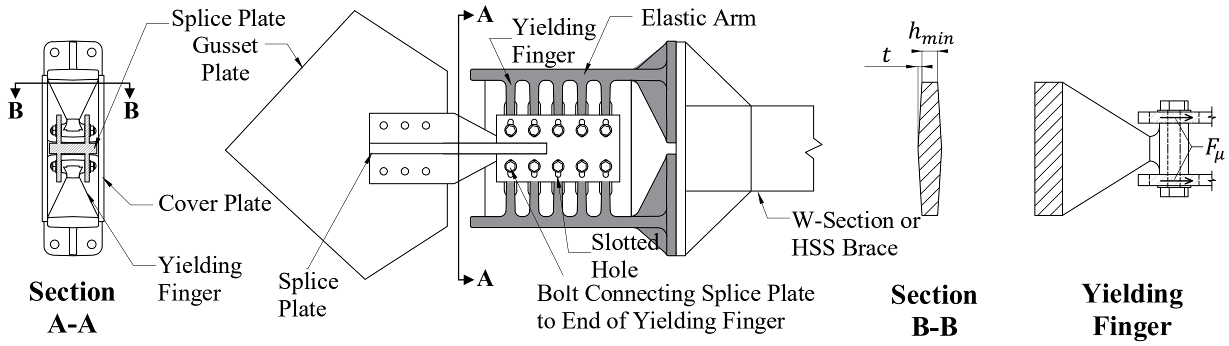

Fig. 1 – Cast Steel Yielding Connector

2. ULCF Fracture Model

One typical ultimate limit state of ductile steel structural element under earthquake loading is the ULCF fracture, which is caused by the micromechanical mechanism of voids nucleation, growth, and coalescence. Research has shown that two important stress-state parameters can be used to numerically express the ductile fracture process: the stress triaxiality and the Lode angle parameter, which are referred to as the tensile and shear fracture parameters, respectively [7, 8, 9, 10, 11, 12, 13, 14, 15]. Since then, various ULCF fracture criteria have been developed with which the ductile fracture demand is calculated based on the stress triaxiality and the Lode angle parameter. This study briefly presents one state-of-the-art ULCF fracture criteria, the Stress Weighted Damage Model (SWDM), previously calibrated by Zhong et al. [4] to the cast steel YC.

2.1 ULCF Fracture Criteria and Calibration

The calibrated SWDM for cast steel YCs was originally proposed by Smith et al. [10] for rolled steel. The fracture criterion of the SWDM is expressed in Eq. (1) as:

$$D_{SWDM} = e^{\lambda \cdot \varepsilon_{acc}} \times \int_{loading} (e^{C_2 \times T} - e^{-C_2 \times T}) \cdot e^{\kappa |X|} \cdot d\varepsilon^p \geq D_{SWDM}^{critical} \tag{1}$$

where λ is a material constant characterizing the rate of cyclic deterioration of the monotonic capacity; ε^p is the equivalent plastic strain for damage measure during repeated loadings. The integrand in the SWDM criterion accounts for a lower damage rate under lower triaxiality to acknowledge experimental results by Bridgeman [16] and Smith et al. [11]. The effect of the Lode angle parameter on the change in damageability, which has been found to strongly influence the ULCF fracture especially in the low triaxiality range, is expressed the natural logarithm of $\kappa|X|$, where X is the Lode angle parameter calculated as $3\sqrt{3} \cdot J_3/(2 \cdot J_2^{3/2})$ and κ is an adjustable coefficient controlling the change in damageability with respect to the Lode angle parameter. J_2 and J_3 are the second and third invariants of the deviatoric stress tensor.

The SWDM is dependent on three key parameters: $D_{SWDM}^{critical}$, λ and κ. $D_{SWDM}^{critical}$ is typically calibrated by monotonic cylindrically notched tension coupon specimens (CNTs) tests, while the calibration of λ requires a set of cyclic CNTs tests of various loading protocols. These CNTs are tested up to failure and are numerically replicated to extract corresponding stress and strain quantities at the instant of fracture. These stress and strain quantities then provide data for curve-fitting into an exponentially decreasing function in order to determine the value of $D_{CVGM}^{critical}$ and λ. The value of κ is calibrated by monotonic tests of coupons with notch geometries that have varying Lode angle parameters under certain triaxiality values at the location of the fracture.

Numerical replication of coupon test results requires an accurate material model for the cast steel specimens. The Armstrong-Frederick (A-F) constitutive model [17] is selected to simulate the material hardening behavior of the cast steel specimens which considers nonlinear combined isotropic and kinematic hardening. This model has been shown to be versatile in modeling steel structures subjected to reverse cyclic loadings. A total of 18 coupon tests are performed by Zhong et al. [4] for the calibration of the cast steel material. The A-F constitutive model is calibrated using an automated optimization algorithm to minimize error between test results and finite element simulations of the load-deformation responses of coupon specimens [18], while the SWDM is calibrated using a device-specific ULCF model calibration process to improve the accuracy of the model for a set number of coupons [4].

2.2 Post-Fracture Modelling of YC

The calibrated SWDM is validated against nine full-scale experimental results that shows predicted fractures of full-scale YC specimens within one cycle of the experimentally defined failure for most loading protocols, and the predicted fracture locations agreed well with the experimental observations [4]. However, YC typically exhibited a significant amount of ductility even after local fracture initiation. To address this, Zhong et al. [5] extended the fracture modeling of YC to simulate the entire ductile fracture process of YC, including ductile fracture initiation, propagation and crack closure due to load reversal. The crack simulation procedure follows three main steps: (1) calculating the damage value of every finite element using the calibrated SWDM; (2) modifying the element constitutive model to simulate the crack opening by reducing its load-carrying capacity to a small percentage (i.e. less than 1%) of the unfractured capacity while tracking the displacement of the element after fracture; and (3) modifying the element constitutive model to simulate crack closing by restoring its load-carry capacity when the element is under an overall compressive hydrostatic stress and that the fractured displacement approaches zero. This crack simulation scheme is an extension to the established phase-field approach which simulates the fracture process by updating continuous field variables whose value indicates the damage state of the finite element [19, 20, 21, 22, 23, 24]. By simulating cracks with a diffusive crack zone instead of establishing crack surfaces, this approach is effective in modeling complicated fracture process especially in 3D or multi-crack cases.

2.3 Fracture Prediction of Full-Scale Experimental Results

The calibrated SWDM and crack simulation scheme are evaluated against full-scale YC experimental results by Zhong et al. [4, 5]. In this section, a few of previous test results and numerical simulations are presented in Fig. 2 to show the performance of the calibrated FE model. As shown in Fig. 2, the calibrated FE model was able to closely-predict the load-deformation responses of coupon specimens under monotonic and cyclic loadings up to complete fracture, as well as both the pre-fracture hysteretic responses and post-fracture load degradations of full-scale YC specimens tested in a braced frame configuration under axial deformation and in-plane brace rotations.

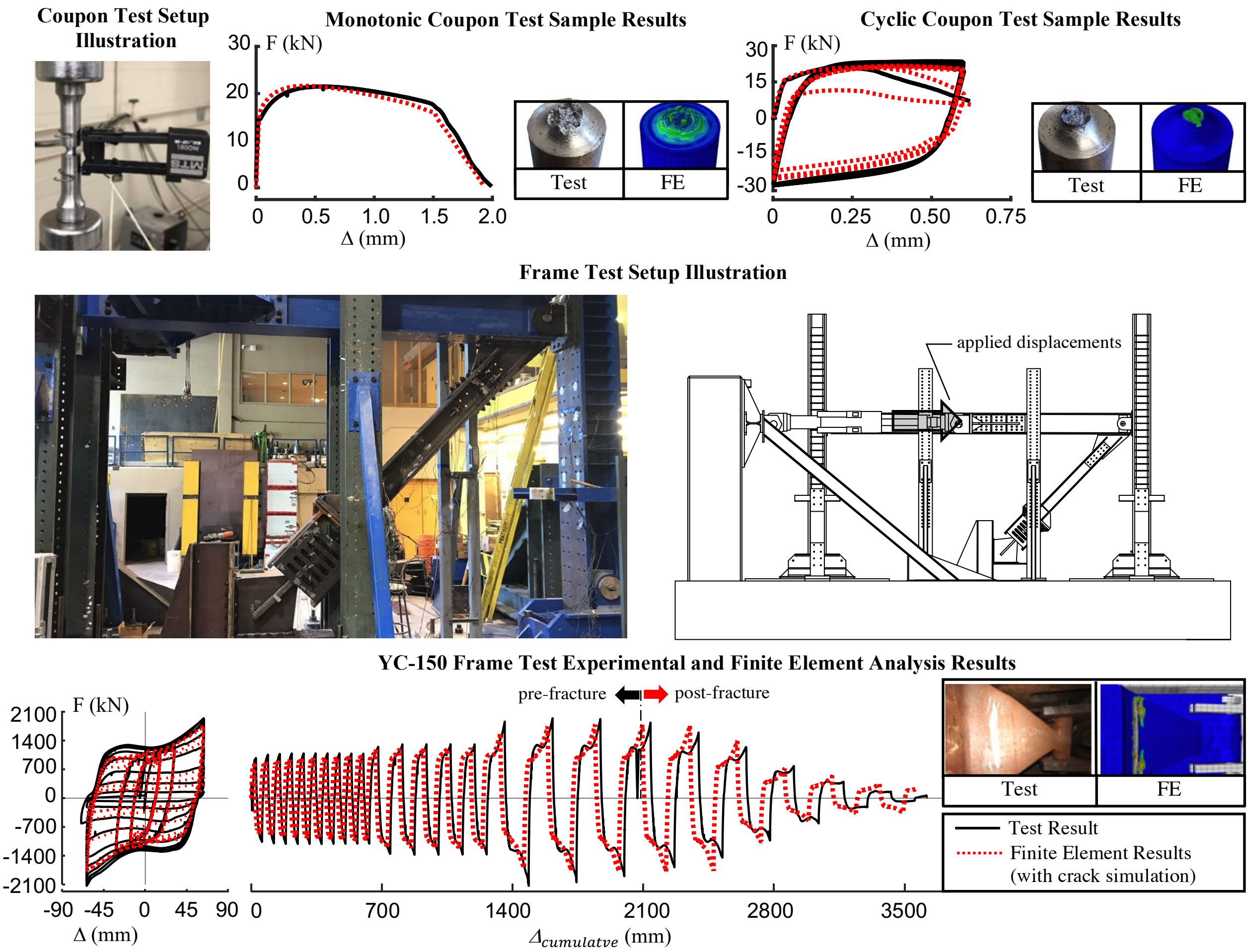

Fig. 2 – Selected Results of the Calibrated FE Model

3. Seismic Performance of Sample Building Structures

Using the calibrated SWDM and the crack simulation scheme that was developed, this paper presents an exploratory study on the effect of the post-yielding response and gradual capacity degradation on the post-fracture performance of non-buckling concentrically braced frames equipped with the cast steel YC.

3.1 Design of Sample Building Structures

The sample structure illustrated in Fig. 3. is a six-story office building designed for normal occupancy in Vancouver, British Columbia, Canada, with a Class D soil profile type in the 2015 National Building Code of Canada (NBCC) [25] and the design provisions for steel structures in CSA S16-19 [26].

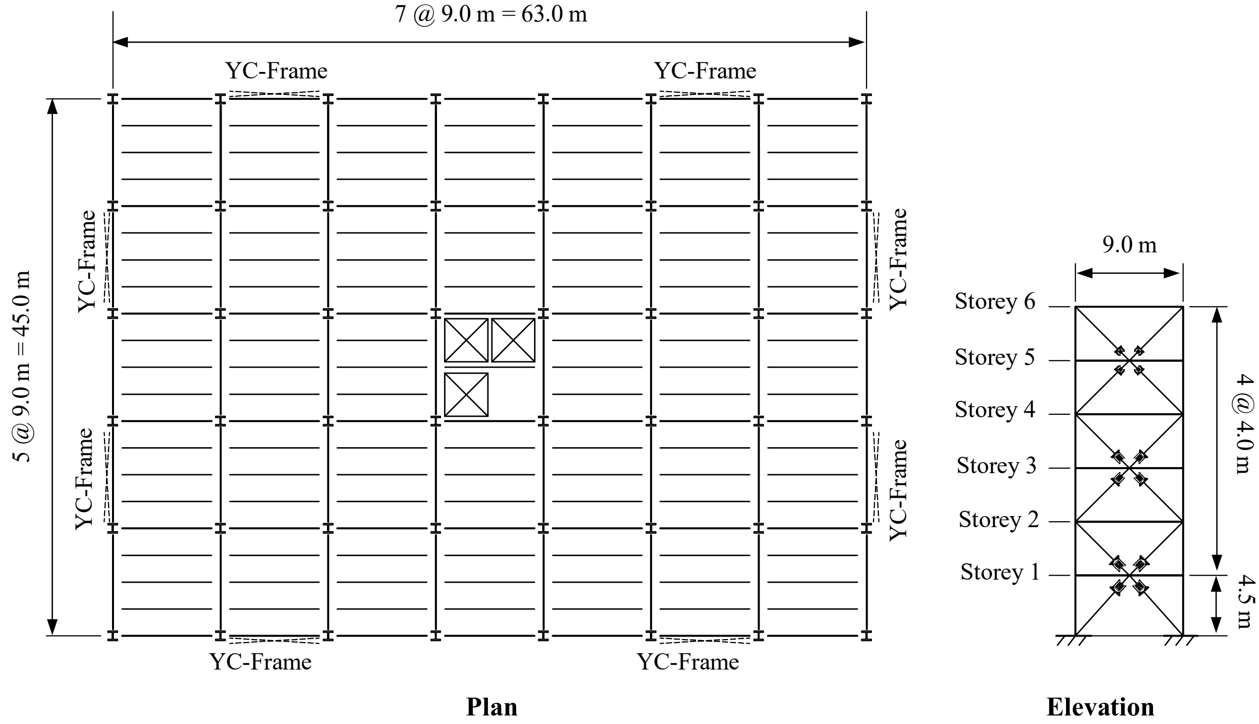

Fig. 3 – Sample Building Layout with YC-Braced Frames

The design spectral accelerations for the sample structure is defined by the following parameters: $S_a(0.2)$ = 1.045, $S_a(0.5)$ = 0.754, $S_a(1.0)$ = 0.394, $S_a(2.0)$ = 0.197, and $S_a(4.0)$ = 0.099. The Seismic Force Resisting System (SFRS) in this building is designed with YC-braced frames based on a modal response spectrum analysis.

The YC-braced frame is proportioned using a methodology analogous to the provisions of AISC 341-16 [27] for Buckling Restrained Braces (BRB). YCs were selected based on strength requirements from pre-engineered connector sizes provided by the manufacturer. The rest of the structural components were designed based on a capacity design approach to resist resultant demands from the adjusted strength of each of the selected YCs, which was approximately 2.1 times the nominal yield strength in general. The resulting member sizes of the YC-braced frame is summarized in Table 1.

Table 1 – YC-Braced Frame Design

Story	YC Nominal Yield Strength [MPa]	Braces	Beams	Columns
6th	517	W250x73	W460x52	W360X147
5th	689	W250x73	W460x52	W360X147
4th	827	W310x86	W460x52	W360X287
3rd	1034	W310x86	W460x52	W360X287
2nd	1186	W310x97	W460x52	W360X382
1st	1482	W310x97	W460x52	W360X382

3.2 Finite Element Modelling Scheme

The detailed model was constructed for the YC-braced frame using commercial FE software ABAQUS 6.13 explicit [28]. YCs were modeled with 3D solid elements while the rest of the frame was modeled with stick elements and assumed centerline dimensions, as shown in Fig. 4. Columns were oriented with their strong axis in the direction of the frame and were modeled with the "beam" element and nonlinear material properties. Beams in the YC-braced frame were modeled with the "beam" element with "true pins" at the beam-column intersections. Gussets at both ends of each brace were modeled with the "beam" element. Second-order effects were accounted for in the model by enabling nonlinear geometry option in the analysis and modelling leaning columns. The leaning column was added beside the YC-braced frame and connected to each story of the frame using "truss" elements with an artificially large axial stiffness. The leaning column was pinned at its base such that it does not contribute to the lateral stiffness of the frame. Seismic masses that represented the assumed tributary dead load (1.0D) and 25% of the live load (0.25L) were assigned to each column node, while gravity forces representing the assumed loads of 1.0D and 0.25L in the lateral tributary area of the frame excluding the frame column tributary areas were applied to the leaning column.

The nonlinear behavior of YCs was simulated using the A-F material constitutive model and the SWDM fracture criterion calibrated by Zhong et al. [4] and implemented with the modified ABAQUS subroutine algorithm developed by Zhong et al. [5]. As illustrated in Fig. 4, half of each YC was modeled owing to symmetry in the plane of the frame. The elastic arm and finger bolt holes were modeled with C3D10M tetrahedral elements in ABAQUS that were geometrically versatile to accurately capture the shape of the castings. C3D8R hexahedral elements were used elsewhere for computational efficiency. A refined mesh size of approximately 2 mm was assigned to the yielding finger region, where inelasticity and fracture demands were concentrated. Finger bolts were modeled with three contact interactions assigned between 1) bolt shank and finger bolt hole, 2) bolt shank and splice plate slotted hole, and 3) bolt head and splice plate face. The finger bolt had a refined mesh size of 3 mm while the bolt hole and the slotted hole had a refined mesh size of 6 mm to better capture the slipping, bearing, and deformation in this region. The YCs were connected to the braces through the coupling constraint assuming fixed connections. The YC-brace FE modelling scheme was validated against four full-scale YC-braced frame tests results (see Fig. 2 for one of the tests and FE simulation results) in Zhong et al. [5] and showed a close match between the pre-fracture hysteretic responses and post-fracture load degradations for all four YC-brace tests.

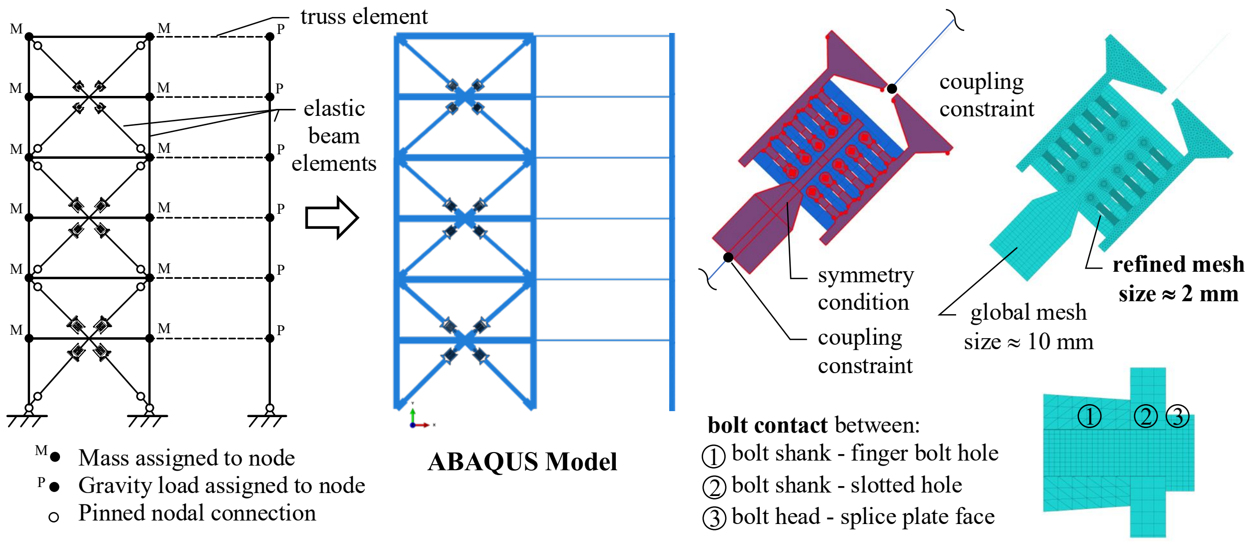

Fig. 4 – YC-Braced Frames Finite Element Model Schematics

The frame model was pinned at its base and was restricted from out-of-plane displacement. A series of ground motions were applied at the base of the frame for time-history analyses. The model included 2.5% Rayleigh damping in the first and third modes. A suite of eleven ground motion records was obtained from the PEER Ground Motion Database [29] and linearly scaled according to the requirement of ASCE 7-16 [30] to have a 2% probability of being exceeded in 50 years (maximum probable earthquake), were used in the time-history analysis, as summarized in Table 2.

Table 2 – Suite of Eleven Ground Motion Records

No.	Earthquake	Recording Station	M[1]	Scaling Factor	PGA[2]
1	Superstition Hills (1987)	Parachute Test Site	6.54	1.34	0.432
2	Northridge (1994)	Sylmar - Converter Station	6.69	2.11	0.623
3	Loma Prieta (1989)	Saratoga - Aloha Ave	6.93	1.26	0.514
4	Landers (1992)	Yermo Fire Station	7.28	2.25	0.245
5	Kocaeli (1999)	Izmit	7.51	1.51	0.230
6	Duzce (1999)	Duzce	7.14	0.96	0.404
7	Denali (2002)	TAPS Pump Station	7.9	4.8	0.075
8	Imperial Valley (1979)	EI Centre	6.53	1.64	0.317
9	Irpinia (1980)	Sturno	6.90	1.26	0.227
10	Chi-Chi (1999)	CHY006	7.62	1.26	0.359
11	Christchurch (2011)	Christchurch	6.20	0.98	0.371

[1]Magnitude
[2]Peak ground acceleration

3.3 Discussion on Analysis Results

The YC-braced frame model was subjected to the scaled suite of records in Table 2. The peak and residual inter-story drift ratios, peak absolute accelerations, and maximum storey shears are presented in Fig. 5 for all eleven ground motions. In general, inelastic demands were higher on the lower stories of the frame. The sample building had mean peak interstorey drift of less than 3.5%, mean residual interstorey drift of less than 2%, mean peak absolute acceleration of 0.67 g, and a mean base shear of 2,438 kN. None of the analyses were found to have ULCF fracture initiated in the YC, based on the calibrated SWDM model.

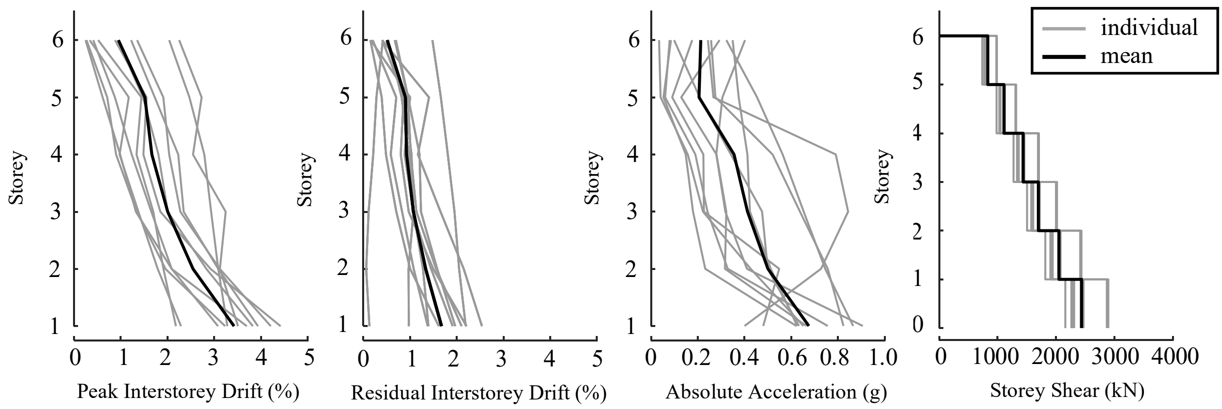

Fig. 5 – Time-History Responses Envelope

To further examine the potential effects of the post-yielding response and gradual capacity degradation of YC on the ultimate response of the structure, the designed YC-braced frame model was subjected to consecutive ground motions scaled from the Kocaeli record (see Table 2) as shown in Fig. 6(a). The first ground motion was scaled to the design basis earthquake (DBE) level with a 10% probability of being exceeded in 50 years. The rest of the ground motions were scaled to represent the effect of maximum considered earthquakes (MCE) with a 2% probability of being exceeded in 50 years.

As indicated in Fig 6(a), the designed YC-braced frame model survived the DBE earthquake and three consecutive MCE earthquakes with minor cracking initiated in YCs and strength degradation. The first onset of ULCF fracture occurs in the 1st storey YCs where inelastic demands were concentrated on. Because of the post-fracture stiffness increase and gradual strength degradation, the 1st storey YCs were able to continue carrying a significant amount of demands. Prior to the complete fracture of a few YC fingers in the 1st storey, crack initiated in the 2nd, 3rd and 5th storey at similar analysis time, followed by crack imitation in the 4th and 6th storey YCs. During the 4th MCE earthquake loading, approximately one-third of the yielding fingers in the 1st storey YCs were fractured completely, leading to a significant amount of load degradation. The first large pulse of the 5th MCE earthquake loading fractured all of the yielding fingers in the 1st storey YCs and multiple complete yielding finger fractures in the 2nd, 3rd and 5th storey YCs. The 4th and 6th storey YCs were also severely damaged but no complete finger fractures were observed. Up to the complete failure of 1st storey YCs, no excessive demand was observed in the rest of the frame outside the YCs. The hysteretic response of individual YC elements further confirmed its post-fracture performance. To illustrate, the entire responses of the two 1st storey YCs until complete fracture are presented in Fig. 6(b), along with the corresponding uncracked and fully cracked deformed shapes at 126 seconds and 324 seconds of the analysis time, respectively.

In this analysis, connection details and other elements of the frame were modeled elastically in order to focus on the performance of the YC-braced frame with respect to collapse due to ULCF fractures. Maximum resultant forces in each member were checked against code prescribed capacities in CSA S16-19 [26] to ensure ULCF fractures initiated prior to reaching limit states for frame members such as the compressive buckling of braces and columns, and the flexural yielding of beams and columns. However, other potential failure modes, such as gusset buckling and fracture of connections, were not considered in this frame model. While the analysis was limited to simulating the progressive collapse of a YC-braced frame triggered by ULCF fractures within YCs, the results of this study, and future more thorough investigations, can be used to inform the capacity design forces used to design the capacity protected elements in YC-braced frames.

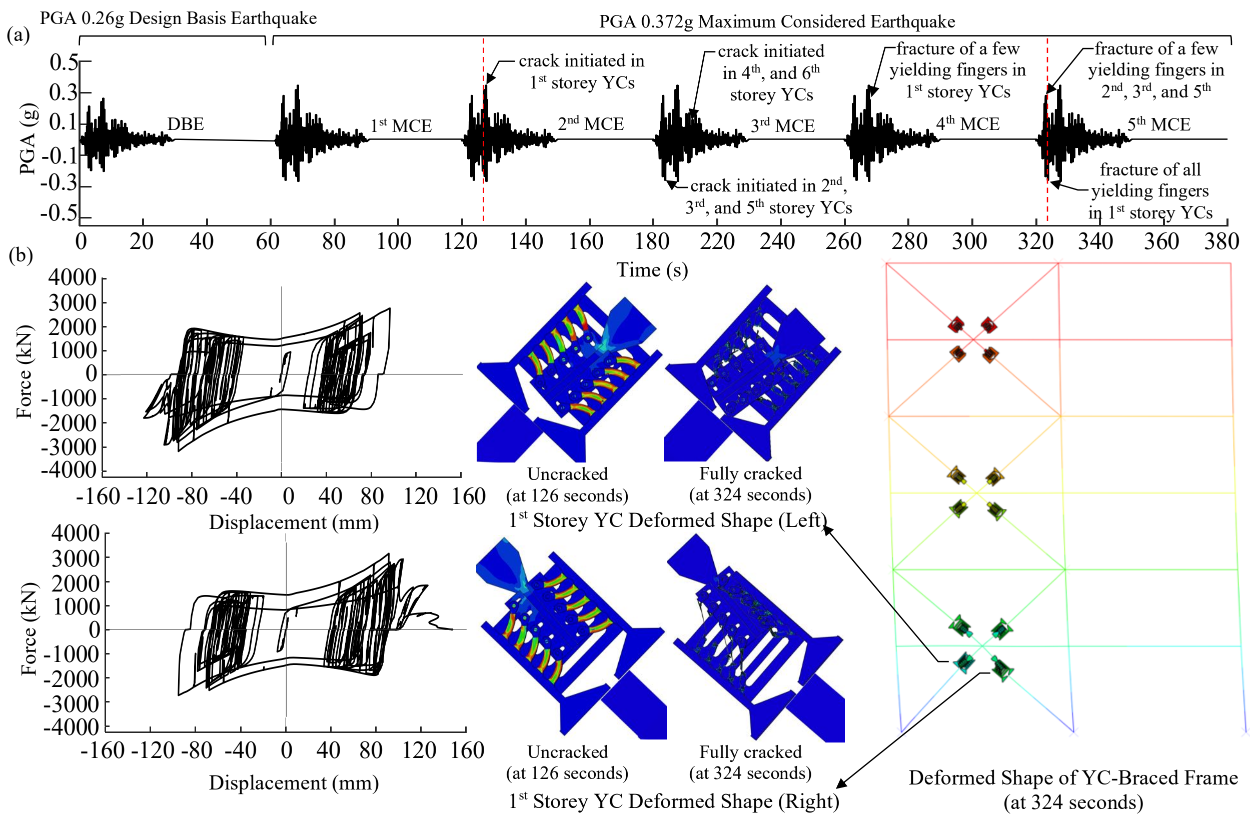

Fig. 6 – Time-History Performance Assessment Results

4. Conclusions

This paper presents the FE modeling and time-history analysis of a six-story sample building designed with YC- braces. A calibrated ULCF fracture criterion and a crack propagation simulation model were used to investigate the post-fracture performance of the YC-braced frame in an exploratory numerical study. Results indicated a promising post-fracture collapse-resistance performance of the structure, due to YC's characteristic post-yield stiffness increase prior to fracture and the gradual load degradation after fracture initiated. Future studies are suggested to validate the calibrated ULCF fracture criterion and the developed crack propagation simulation model against full-scale experimental results under earthquake excitations and to evaluate the post-fracture performance of YC-equipped buildings with various sizes.

5. Acknowledgments

The financial support of the Ontario Centres of Excellence (OCE) and Natural Sciences and Engineering Research Council (NSERC) is gratefully acknowledged. Any opinions, findings, and conclusions or recommendations expressed in this material are those of the authors and do not necessarily reflect the views of the OCE and NSERC.

6. References

[1] Gray, M. G., Christopoulos, C., & Packer, J. A. (2013): Cast Steel Yielding Brace System for Concentrically Braced Frames: Concept Development and Experimental Validations. *Journal of Structural Engineering*, **140** (4), 04013095

[2] Gray, M. G., Christopoulos, C., & Packer, J. A. (2016): Design and Full-Scale Testing of a Cast Steel Yielding Brace System in a Braced Frame. *Journal of Structural Engineering*, **143** (4), 04016210.

[3] Martyr, R., & Christopoulos, C. (2018): Applying the Cyclic Void Growth Model to Assess the Ultralow Cycle Fatigue Life of Steel Castings. *Journal of Structural Engineering*, **144** (8), 04018129.

[4] Zhong, C., Binder, J., Kwon, O. S., & Christopoulos, C. (2019): Experimental and Numerical Characterization of Ultralow-Cycle Fatigue Behavior of Steel Castings. *Journal of Structural Engineering*, **146** (2), 04019195.

[5] Zhong, C., Binder, J., Kwon, O. S., & Christopoulos, C. (2020): Full-Scale Experimental Testing and Post-Fracture Simulation of the Cast Steel Yielding Connector. *Journal of Structural Engineering*, Manuscript submitted for review.

[6] Mortazavi, P., Gray, M., Kwon, O., and Christopoulos, C. (2020): Four-Element Hybrid Simulation of a Steel Frame with Cast Steel Yielding Braces," *17th World Conference on Earthquake Engineering*, Sendai, Japan, September 13-18. (submitted)

[7] Kanvinde, A. M., and G. G. Deierlein. (2006): Void Growth Model and Stress Modified Critical Strain Model to Predict Ductile Fracture in Structural Steels. *Journal of Structural Engineering*, **132** (12): 1907-1918.

[8] Myers, A. T., G. G. Deierlein, and A. M. Kanvinde. (2009): Testing and Probabilistic Simulation of Ductile Fracture Initiation in Structural Steel Components and Weldments. *Technical Report 170*, John A. Blume Earthquake Engineering Centre, Stanford University, Stanford, CA.

[9] Hommel, J. H., & Meschke, G. (2010): A Hybrid Modeling Concept for Ultra Low Cycle Fatigue of Metallic Structures based on Micropore Damage and Unit Cell Models. *International Journal of Fatigue*, **32** (12), 1885-1894.

[10] Martinez, X., Oller, S., Barbu, L. G., Barbat, A. H., & De Jesus, A. M. P. (2015): Analysis of Ultra Low Cycle Fatigue Problems with the Barcelona Plastic Damage Model and a New Isotropic Hardening Law. *International Journal of Fatigue*, **73**, 132-142.

[11] Smith, C. M., Deierlein, G. G., and Kanvinde, A. M. (2014): A Stress Weighted Damage Model for Ductile Fracture Initiation in Structural Steel under Cyclic Loading and Generalized Stress States. *Technical Report 187*, Blume Earthquake Engineering Center, Stanford University, Stanford, CA.

[12] Kiran, R., & Khandelwal, K. (2015): A Micromechanical Cyclic Void Growth Model for Ultra-low Cycle Fatigue. *International Journal of Fatigue*, **70**, 24-37.

[13] Tong, L., Huang, X., Zhou, F., & Chen, Y. (2016): Experimental and Numerical Investigations on Extremely-Low-Cycle Fatigue Fracture Behavior of Steel Welded Joints. *Journal of Constructional Steel Research*, **119**, 98-112.

[14] Wen, H., and H. Mahmoud. (2016): New Model for Ductile Fracture of Metal Alloys. II: Reverse Loading. *Journal of Engineering Mechanics*, **142** (2): 4015089.

[15] Algarni, M., Choi, Y., & Bai, Y. (2017): A Unified Material Model for Multiaxial Ductile Fracture and Extremely Low Cycle Fatigue of Inconel 718. *International Journal of Fatigue*, **96**, 162-177.

[16] Bridgman, P. W. (1964): *Studies in Large Plastic Flow and Fracture*. Cambridge, MA: Harvard University Press.

[17] Armstrong, P. J., and Frederick, C. O. (1966): A Mathematical Representation of the Multiaxial Bauschinger Effect. Berkeley Nuclear Laboratories, Research and Development Department, Berkeley, U.K.

[18] Smith, C., A. Kanvinde, and G. Deierlein. (2017): Calibration of Continuum Cyclic Constitutive Models for Structural Steel using Particle Swarm Optimization. *Journal of Engineering Mechanics*, **143** (5): 04017012.

[19] Francfort, G. A., & Marigo, J. J. (1998): Revisiting Brittle Fracture as An Energy Minimization Problem. *Journal of the Mechanics and Physics of Solids*, **46** (8), 1319-1342.

[20] Borden, M. J., Verhoosel, C. V., Scott, M. A., Hughes, T. J., & Landis, C. M. (2012): A Phase-Field Description of Dynamic Brittle Fracture. *Computer Methods in Applied Mechanics and Engineering*, **217**, 77-95.

[21] Borden, M. J., Hughes, T. J., Landis, C. M., Anvari, A., & Lee, I. J. (2016): A Phase-Field Formulation for Fracture in Ductile Materials: Finite Deformation Balance Law Derivation, Plastic Degradation, and Stress Triaxiality Effects. *Computer Methods in Applied Mechanics and Engineering*, **312**, 130-166.

[22] Ambati, M., Gerasimov, T., & De Lorenzis, L. (2015): Phase-Field Modeling of Ductile Fracture. *Computational Mechanics*, **55** (5), 1017-1040.

[23] Ambati, M., Gerasimov, T., & De Lorenzis, L. (2015): A Review on Phase-Field Models of Brittle Fracture and a New Fast Hybrid Formulation. *Computational Mechanics*, **55** (2), 383-405.

[24] Ambati, M., Kruse, R., & De Lorenzis, L. (2016): A Phase-Field Model for Ductile Fracture at Finite Strains and its Experimental Verification." Computational Mechanics, **57** (1), 149-167.

[25] NRCC (National Research Council Canada). (2015): *National Building Code of Canada*, 14th Ed., Ottawa.

[26] CSA (Canadian Standards Association). (2019): *Limit States Design of Steel Structures*. CAN/CSA-S16-19, Mississauga, ON, Canada.

[27] American Institute of Steel Construction (AISC): *ANSI/AISC 341-16 Seismic Provisions for Structural Steel Buildings*. AISC: Chicago, 2016.

[28] ABAQUS/CAE 6.13-1 [Computer software] (2013): Systèmes, Vélizy-Villacoublay, France.

[29] Pacific Earthquake Engineering Research Center (PEER) (2013): *PEER Ground Motion Database Web Application*. University of California, Berkeley, CA.

[30] American Society of Civil Engineers (ASCE)/Structural Engineering Institute (SEI) (2016): *ASCE/SEI 7-16 Minimum Design Loads for Buildings and Other Structures*. ASCE/SEI: Reston, 2016.

